EXPERIMENTAL INVESTICATIONS ON MOLECULAR STRUCTURE VIBRATIONAL SPECTRA, MULLIKEN ATOMIC CHARGE, AND HOMO-LUMO, ANALYSIS OF 4-(PHENYLMETHYL) PHENOL.

T. Rajalakshmy[1], S. Saravanan[2], D.Henry Raja[1*], V. Balachandran[3]

[1]Department of Physics and Research Centre, Scott Christian College, Nagercoil 629 003, India

[2]PG and Research Department of Physics, National College (Auto.), Tiruchirappalli 620 001, India

[3]Centre for research, Department of Physics, A A Government Arts College, Musiri, Tiruchirappalli 621 211, India

Abstract

The FT-IR Raman spectra of 4-(phenylmethyl) phenol (4PMP) have been recorded in the region 4000-400 cm^{-1} and 3500-100cm^{-1} respectively. The total energy calculations of 4pmp were tried for the possible conformers. The molecular structure, geometry optimization, vibrational frequencies were obtained by the density functional theory (DFT) using B3LYP method with 6-31+G (d) and 6311++G (d, p) basis sets. The complete assignments were performed on the basis of the potential energy distribution (PED) of the vibrational modes, calculated and the scaled values were compared with experimental FT-IR and FT-RAMAN spectra. The observed and the calculate frequencies are found to be in good agreement. A Mulliken's atomic charge analysis has also been made on optimized geometries of 4pmp in gas phase. Information about the size, shape charge density distribution and site of decimal respectively of the molecules has been obtained by mapping electron density surface with molecular electrostatic potential (MEP).

KEYWORDS:

DFT calculations

FT-IR spectra

FT-Raman spectra

HOMO-LUMO

* Corresponding author. Tel.: +91 9488748900.

E-mail address: henry_raja@yahoo.co.in. (D. HENRY RAJA)

I. INTRODUCTION

The electro negative atom such as halogen attached to the (phenymethyl) phenol in a highly reactive the phenyl methylphenol. The 4-(phenylmethyl) phenol is a white crystalline powder with molecular formula $(Cl_3H_{12}O)$.The vibration spectroscopic using DFT methods have reported on methyl phenol. Therefore the present investigation was undertaken study the vibration of FT-IR, FT-Raman spectra of the molecule completely and to identify the vibrations normal modes with grater wave number accuracy. Predication of vibration frequency of polyatomic molecules by quantum chemical calculation has become very popular because of accurate and consistent description of the experimental data. 4pmp was investigated by using B3LYP calculation with 6-31+G (d) and 6-311++G (d, p) basis sets.

II. EXPERIMENTAL DETAILS

The pure sample of 4PMP in the light yellow waxy solid form was purchased from the Lancaster Chemical Company (UK), with a stated purity of greater than 98% and it was used as such without further purification. The FT-IR spectrum of this compound was recorded in the region 4000−400 cm^{-1} on IFS 66V spectrometer equipped with an MCT detector using KBr beam splitter and globar source. The FT-Raman spectrum of title molecule has been recorded using the 1064 nm line of a Nd:YAG laser as excitation wavelength in the region 3500−100 cm^{-1} on a BRUKER model RFS 66V spectrometer. The reported wavenumbers are expected to the accurate within ±1 cm^{-1} resolution with 250 mW of power at the sample in both the techniques.

III. COMPUTATIONAL DETAILS

The entire calculations was performed at DFT/B3LYP method with 6-31+G(d) and 6-31++G(d, p) levels with the standard basis set 6-311G++ (d, p) on personal computer using GAUSSIAN 09W [1] program package, invoking gradient geometry optimization [2]. The global minimum energy conformer is used in the vibrational wavenumber calculation at the B3LYP and with using 6-311G (d, p) level. Subsequently, the vibrational in association with the molecule were derived along with their IR intensity and Raman activity. In order to fit the theoretical wavenumbers to the experimental, the scaling factors have been introduced by using a least square optimization method. The polarizability, hyperpolarizability and dipole moments of 4PMP have been calculated using the same method. The HOMO−LUMO analysis has been carried out to explain the charge transfer within the molecule. The global hardness (η), global softness (υ), electronegativity (χ) and chemical potential (μ) have been calculated using the highest occupied molecular orbital (HOMO) and lowest unoccupied molecular orbital (LUMO). The natural bonding orbital's (NBO) calculations [3] were performed using NBO 3.1 program as implemented in GAUSSIAN 09W package at DFT level in order to understand various second order interactions between the another subsystem, which is a measure of the intramolecular delocalization or hyper-conjugation. To check whether the chosen set of symmetric coordinates contribute maximum to the potential energy associated with the molecule, the PED has been carried out. The transformation of force field, subsequent normal coordinate analysis and calculation of the PED were done on a PC with the MOLVIB program (Version 7.0 – G77) written by Sundius [4]. The complete information's regarding population of electrons in sub-shells of atomic orbital's and electron densities of an atom in the title molecule.

Prediction of Raman Intensity

The Raman activities (S_i) calculated with the GAUSSIAN 09W Program were converted to Raman intensities (I_i) using the following relationship derived from the intensity theory of Raman scattering [5, 6].

$$I_i = \frac{f(\upsilon_0 - \upsilon_i)^4 S_i}{\upsilon_i[1 - \exp(-hc\upsilon_i/kT)]}$$

where υ_0 is the laser exciting frequency in cm^{-1} (in this work, we have used the excitation wavenumber υ_0=9398.5 cm^{-1}, which corresponds to the wavelength of 1064 nm of a Nd:YAG laser), υ_i is the vibrational wavenumber of the ith normal mode (in cm^{-1}) and S_i is the Raman scattering activity of the normal mode υ_i, f (is the constant equal to 10^{-12}) is a suitably chosen common normalization factor for all peak intensities. h, k, c, and T are Planck constant, Boltzmann constant, speed of light, and temperature in Kelvin, respectively.
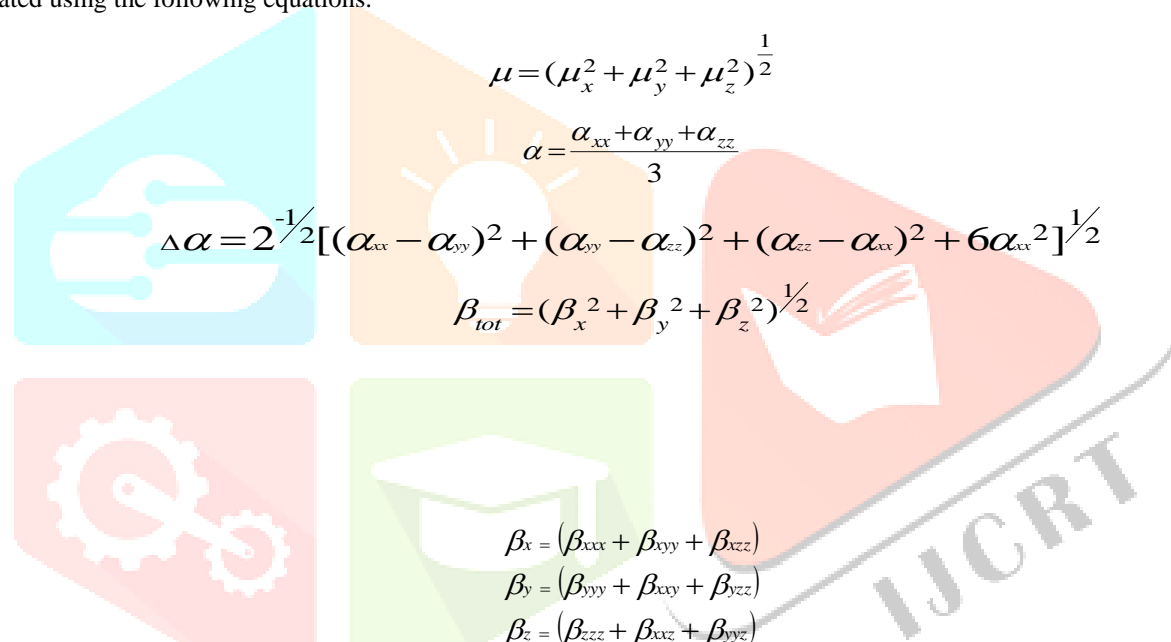
Nonlinear Optical Effects

The nonlinear optical effects arise due to the interactions of electromagnetic fields in various media to produce new fields which are altered in frequency, phase and amplitude or other propagation characteristics from the incident fields [7]. Computational approach is an inexpensive, yet an effective way to design molecules by analyzing their potential which helps to determine the molecular NLO properties. In this direction, quantum chemical calculations of the title compound were carried out using GUASSIAN 09W package employing the B3LYP functional supplemented with standard 6-31+G (d) and 6-311++G(d, p) basis set. The first static hyperpolarizability (β_{tot}) and its related properties (α, β and $\Delta\alpha$) of 4PMP have been calculated using B3LYP/6-31+G (d, p) and /6-311++G (d, p) methods based on finite-field approach and are presented in Table 1. To calculate all the electric dipole moment and the first hyperpolarizability tensor components for a given system will depend on the choice of the Cartesian co-ordinate system (x, y, z)=(0, 0, 0) was chosen at own centre of mass of molecule. The polarizability of this novel molecular system for which $\alpha_{xx} = \alpha_{yy} = \alpha_{zz}$ is said to be isotropic. The polarizability is isotropic or is the same in all directions for a molecular system whose electron density is spherically symmetrical. If the molecule is perfectly isotropic (P) and (E) will have

the same direction and is then a simple scalar quantity. The polarizability of this novel molecular system for which $\alpha_{xx} \neq \alpha_{yy} \neq \alpha_{zz}(P)$ will no longer have the same direction as (E).

In the presence of an applied electric field, the energy of a system is a function of the electric field and the first order hyperpolarizability is a third rank tensor that can be described by a 3×3×3 matrices. The 27 components of the 3D matrix can be reduced to 10 components because of the Kleinman symmetry [8]. It can be given in the lower tetrahedral format. It is obvious that the lower part of the 3×3×3 matrices is tetrahedral. The components of β are defined as the coefficients in the Taylor series expansion of energy in an external electric field. The external electric field is weak and homogeneous, this expansion becomes

$$E = E^0 - \frac{\mu_i F_i}{1!} - \frac{\alpha_{ij} F_i F_j}{2!} - \frac{\beta_{ijk} F_i F_j F_k}{3!} - \frac{\gamma_{ijkl} F_i F_j F_k F_l}{4!} + \cdots$$

where E^0 is the energy of the unperturbed molecules, F_i is the field at the origin and μ_i, α_{ij}, β_{ijk} and γ_{ijkl} are the components of dipole moment, polarizability and the hyperpolarizability, respectively. The total static dipole moment (μ), the mean polarizability (α), the anisotropy of the polarizability ($\Delta\alpha$) and the mean first hyperpolarizability (β_{tot}), using the x, y, z components can be calculated using the following equations:

$$\mu = (\mu_x^2 + \mu_y^2 + \mu_z^2)^{\frac{1}{2}}$$

$$\alpha = \frac{\alpha_{xx} + \alpha_{yy} + \alpha_{zz}}{3}$$

$$\Delta\alpha = 2^{-\frac{1}{2}}[(\alpha_{xx} - \alpha_{yy})^2 + (\alpha_{yy} - \alpha_{zz})^2 + (\alpha_{zz} - \alpha_{xx})^2 + 6\alpha_{xx}^2]^{\frac{1}{2}}$$

$$\beta_{tot} = (\beta_x^2 + \beta_y^2 + \beta_z^2)^{\frac{1}{2}}$$

where

$$\beta_x = (\beta_{xxx} + \beta_{xyy} + \beta_{xzz})$$
$$\beta_y = (\beta_{yyy} + \beta_{xxy} + \beta_{yzz})$$
$$\beta_z = (\beta_{zzz} + \beta_{xxz} + \beta_{yyz})$$

Since the values of the polarizabilities ($\Delta\alpha$) and the hyperpolarizabilities (β_{tot}) of the GAUSSIAN 09 output are obtained in atomic units (a.u.), the calculated values have been converted into electrostatic units (e.s.u.) (1 a.u.=8.3693x10^{-33} e.s.u.). The total molecular dipole moment and first order hyperpolarizability are 1.4985and 1.4792 Debye, and 0.508×10^{-30}and 0.545x10^{-30} e.s.u., respectively and are depicted in Table 1. Urea is one of the prototypical molecules used in the study of the NLO properties of molecular systems and frequently used as a threshold value for comparative purposes. First order hyperpolarizability of the title molecule is 1.9 times greater than those of urea (μ and β of urea are 1.3732 Debye and 0.33728x10^{-30} e.s.u.) obtained by B3LYP/6-31+G (d) and /6-311++G (d, p) methods. So we conclude that the title molecule is an attractive object for future studies of non-linear optical properties.

Table 1

The electric dipole moment (μ) (debye), the mean polarizability(α)(e.s.u.), anisotropy polarizability($\Delta\alpha$)(e.s.u.) and first hyperpolarizability(β_{tot})(e.s.u.) for 4-(phenylmethyl)phenol at B3LYP/6-31+G (d) and B3LYP/6-311++G (d, p) methods.

Parameters	B3LYP/6-31+G(d)	B3LYP /6-311++G (d, p)
μ_x	-0.4964	-0.5031
μ_y	-1.3698	-1.3406
μ_z	0.3507	0.3713
μ	1.498584	1.479250
α_{xx}	-85.4695	-85.5969
α_{xy}	-7.3674	-7.2066
α_{xz}	-72.6764	-72.5414
α_{yy}	1.7881	1.8009
α_{yz}	2.2508	2.2003
α_{zz}	-85.1670	-85.0847
A	-81.1043	-81.0743
$\Delta\alpha$	108.9481	109.2749
β_{xxx}	8.6885	8.1131
β_{yyy}	-38.7336	-37.9406
β_{zzz}	11.7980	-11.7155
β_{xyy}	-0.4353	-0.4548
β_{xxy}	-30.4898	-30.0234
β_{xxz}	12.1066	11.8638
B_{xzz}	-3.0099	-2.9319
β_{yzz}	-1.2495	-1.3451
β_{yyz}	-3.4326	-3.3562
β_{xyz}	-2.2405	-2.2374
β_{tot}	0.50832	0.54520

IV. RESULTS AND DISCUSSION

Molecular Geometry

The optimized structural parameters such as bond lengths, bond angles and dihedral angles determined by theoretical B3LYP and methods with 6-31+G (d) and 6-311++G(d, p) basis set. The bond lengths and bond angles and dihedral angles were presented in Table 2 in accordance with the atom numbering scheme as given in Fig. 1.
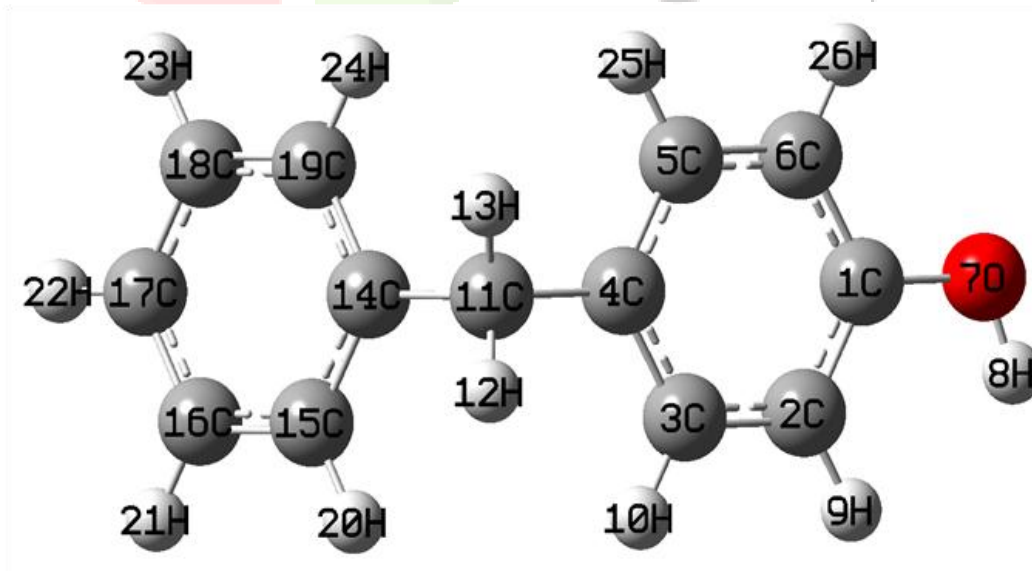

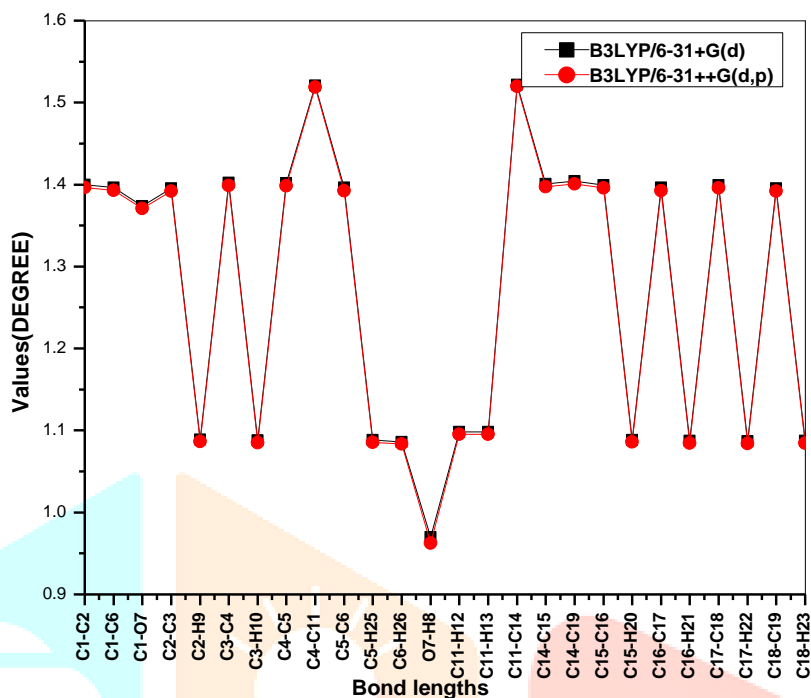Fig.1. Possible conformational structures of 4-(phenylmethyl) phenol

Fig.2. Bond length difference between the theoretical B3LYP/6- 31+G (d) and B3LYP/6-311++G(d, p) of the 4-phenylmethyl) phenol
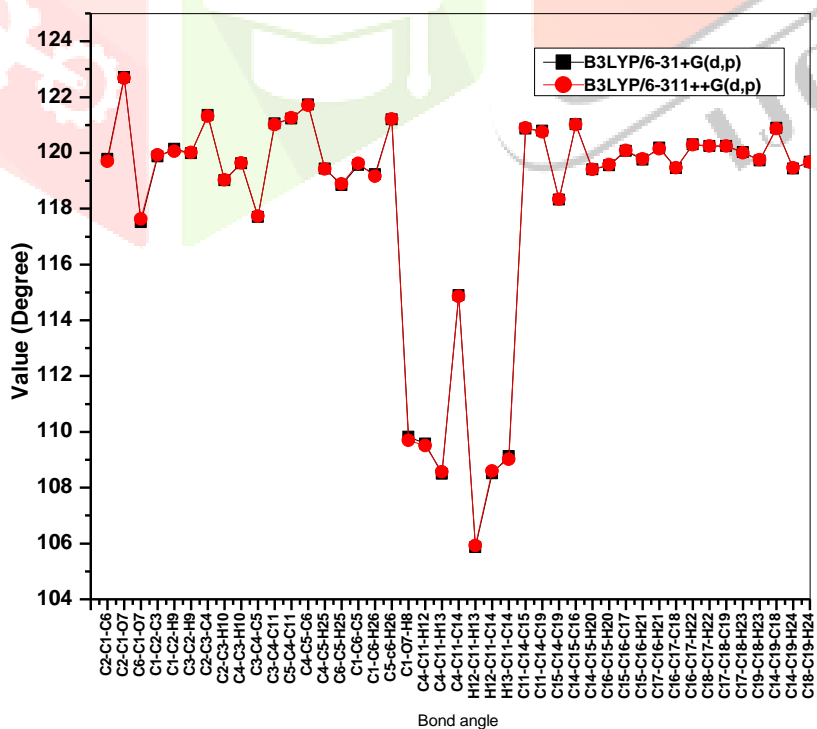

Fig.3. Bond angle differences between experimental and theoretical B3LYP/6-31+G (d) and B3LYP/6-311++G(d, p) of the 4-(phenylmethyl) phenol
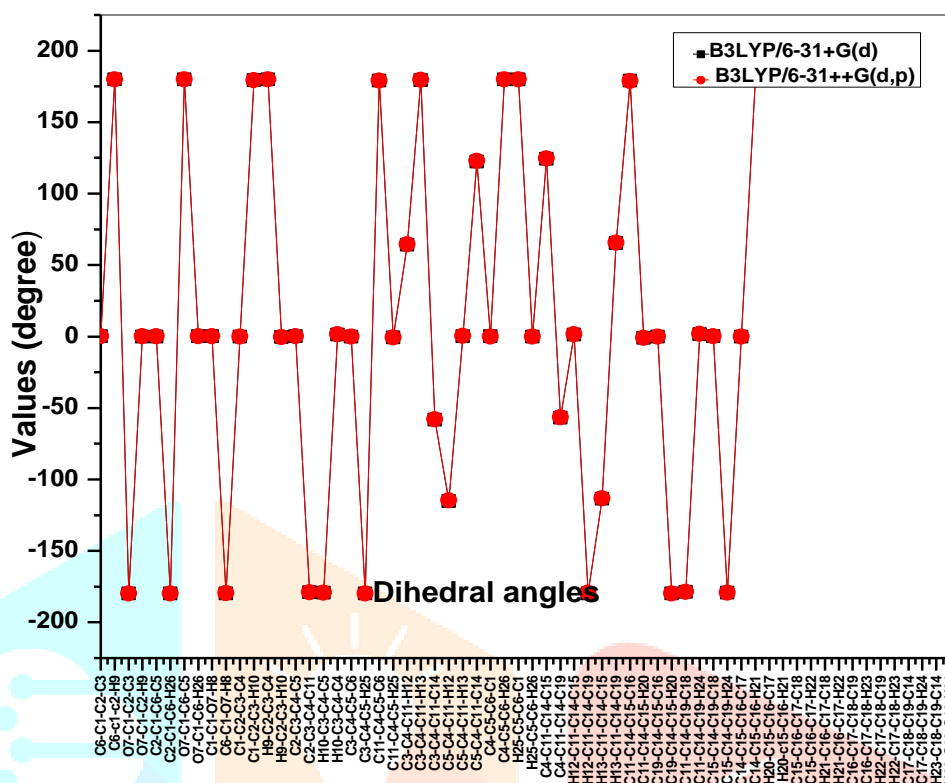
Fig.4. Dihedral angle differences between experimental and theoretical B3LYP/6-31+G(d)and B3LYP/6-311++G(d, p) of the 4-(phenylmethyl) phenol

The computed bond lengths and bond angles are slightly larger and smaller, because the deviation of theoretical calculations are performed upon isolated molecule in the gaseous phase and the experimental results are performed on the solid phase of the molecule. The calculated geometrical parameters by B3LYP/6-31+ G (d) and 6-311++G (d, p) method are very good agreement with method. The C−C aromatic bond distances full in the range from 1.3836 to 1.4057 Å for the B3LYP/6-31+G (d) and 6-311++G (d, p) method, which are in good agreement with those in molecular structure of 4PMP.Figs.2,3,4 respectively.

Table 2

Optimized geometrical metes of 4 (phenylmethyl) phenol by B3LYP/6-31+G (d) and B3LYP/6-311+G (dp) methods.

Bond lengths	Values Å		Bond angles	Values degrees		dihedral angles	Values degrees	
	B3LYP			B3LYP			B3LYP	
	6-31+G (p)	6-311++G (d, p)		6-31+G (p)	6-311++G (d, p)		6-31+G (p)	6-311++G (d, p)
C_1-C_2	1.3997	1.3965	C_2-C_1-C_6	119.78	119.70	C_6-C_1-C_2-C_3	0.08	0.05
C_1-C_6	1.3964	1.3929	C_2-C_1-O_7	122.71	122.67	C_6-c_1-c_2-H_9	179.94	179.93
C_1-O_7	1.3737	1.371	C_6-C_1-O_7	117.52	117.63	O_7-C_1-C_2-C_3	-179.89	-179.88
C_2-C_3	1.3954	1.3917	C_1-C_2-C_3	119.87	119.93	O_7-C_1-C_2-H_9	-0.04	0.01
C_2-H_9	1.0891	1.0864	C_1-C_2-H_9	120.14	120.06	C_2-C_1-C_6-C_5	-0.02	0.05
C_3-C_4	1.4021	1.3986	C_3-C_2-H_9	119.98	120.01	C_2-C_1-C_6-H_{26}	-179.93	-179.90
C_3-H_{10}	1.0878	1.085	C_2-C_3-C_4	121.36	121.32	O_7-C_1-C_6-C_5	179.95	179.98
C_4-C_5	1.4017	1.3982	C_2-C_3-H_{10}	119.01	119.03	O_7-C_1-C_6-H_{26}	0.05	0.03

Bond length		
C_4-C_{11}	1.5208	1.5188
C_5-C_6	1.3962	1.3926
C_5-H_{25}	1.0882	1.0855
C_6-H_{26}	1.086	1.0834
O_7-H_8	0.9698	0.9627
C_{11}-H_{12}	1.0984	1.0954
C_{11}-H_{13}	1.0984	1.0954
C_{11}-C_{14}	1.5218	1.5197
C_{14}-C_{15}	1.401	1.3975
C_{14}-C_{19}	1.4041	1.4007
C_{15}-C_{16}	1.3994	1.3958
C_{15}-H_{20}	1.0885	1.0857
C_{16}-C_{17}	1.3961	1.3922
C_{16}-H_{21}	1.0874	1.0846
C_{17}-C_{18}	1.3995	1.3957
C_{17}-H_{22}	1.0871	1.0842
C_{18}-C_{19}	1.3956	1.3918
C_{18}-H_{23}	1.0874	1.0846
C_{19}-H_{24}	1.0879	1.0851

Bond angle		
C_4-C_3-H_{10}	119.63	119.64
C_3-C_4-C_5	117.70	117.73
C_3-C_4-Cl_1	121.06	121.01
C_5-C_4-C_{11}	121.23	121.25
C_4-C_5-C_6	121.73	121.70
C_4-C_5-H_{25}	119.43	119.42
C_6-C_5-H_{25}	118.84	118.88
C_1-C_6-C_5	119.56	119.62
C_1-C_6-H_{26}	119.23	119.16
C_5-C_6-H_{26}	121.20	121.22
C_1-O_7-H_8	109.82	109.70
C_4-C_{11}-H_{12}	109.58	109.50
C_4-C_{11}-H_{13}	108.49	108.57
C_4-C_{11}-C_{14}	114.90	114.86
H_{12}-C_{11}-H_{13}	105.86	105.92
H_{12}-C_{11}-C_{14}	108.51	108.59
H_{13}-C_{11}-C_{14}	109.13	109.02
C_{11}-C_{14}-C_{15}	120.87	120.90
C_{11}-C_{14}-C_{19}	120.80	120.75
C_{15}-C_{14}-C_{19}	118.32	118.34
C_{14}-C_{15}-C_{16}	121.03	121.01
C_{14}-C_{15}-H_{20}	119.41	119.41
C_{16}-C_{15}-H_{20}	119.55	119.58
C_{15}-C_{16}-C_{17}	120.07	120.08
C_{15}-C_{16}-H_{21}	119.75	119.78
C_{17}-C_{16}-H_{21}	120.18	120.14
C_{16}-C_{17}-C_{18}	119.45	119.46
C_{16}-C_{17}-H_{22}	120.30	120.29
C_{18}-C_{17}-H_{22}	120.25	120.25
C_{17}-C_{18}-C_{19}	120.24	120.24
C_{17}-C_{18}-H_{23}	120.03	120.00
C_{19}-C_{18}-H_{23}	119.73	119.76
C_{14}-C_{19}-C_{18}	120.89	120.87
C_{14}-C_{19}-H_{24}	119.43	119.46
C_{18}-C_{19}-H_{24}	119.68	119.67

Dihedral angle		
C_1-C_1-O_7-H_8	0.13	0.22
C_6-C_1-O_7-H_8	-179.85	-179.70
C_1-C_2-C_3-C_4	-0.17	-0.17
C_1-C_2-C_3-H_{10}	179.41	179.39
H_9-C_2-C_3-C_4	179.98	179.95
H_9-C_2-C_3-H_{10}	-0.45	-0.49
C_2-C_3-C_4-C_5	0.18	0.19
C_2-C_3-C_4-C_{11}	-179.07	-178.96
H_{10}-C_3-C_4-C_5	-179.39	-179.37
H_{10}-C_3-C_4-C_4	1.36	1.48
C_3-C_4-C_5-C_6	-0.12	-0.09
C_3-C_4-C_5-H_{25}	-179.94	-179.96
C_{11}-C_4-C_5-C_6	179.13	179.06
C_{11}-C_4-C_5-H_{25}	-0.69	-0.81
C_3-C_4-C_{11}-H_{12}	64.12	64.45
C_3-C_4-C_{11}-H_{13}	179.25	179.67
C_3-C_4-C_{11}-C_{14}	-58.34	-58.01
C_5-C_4-C_{11}-H_{12}	-115.11	-114.67
C_5-C_4-C_{11}-H_{13}	0.03	0.55
C_5-C_4-C_{11}-C_{14}	122.44	122.87
C_4-C_5-C_6-C_1	0.04	-0.03
C_4-C_5-C_6-H_{26}	179.95	179.92
H_{25}-C_5-C_6-C_1	179.87	179.84
H_{25}-C_5-C_6-H_{26}	-0.23	-0.20
C_4-C_{11}-C_{14}-C_{15}	124.25	124.57
C_4-C_{11}-C_{14}-C_{19}	-56.72	-56.47
H_{12}-C_{11}-C_{14}-C_{15}	1.22	1.62
H_{12}-C_{11}-C_{14}-C_{19}	-179.75	-179.43
H_{13}-C_{11}-C_{14}-C_{15}	-113.68	-113.35
H_{13}-C_{11}-C_{14}-C_{19}	65.35	65.61
C_{11}-C_{14}-C_{15}-C_{16}	178.88	178.85
C_{11}-C_{14}-C_{15}-H_{20}	-0.90	-0.97
C_{19}-C_{14}-C_{15}-C_{16}	-0.16	-0.14
C_{19}-C_{14}-C_{15}-H_{20}	-179.95	-179.96
C_{11}-C_{14}-C_{19}-C_{18}	-178.77	-178.72
C_{11}-C_{14}-C_{19}-H_{24}	1.63	1.71
C_{15}-C_{14}-C_{19}-C_{18}	0.28	0.26
C_{15}-C_{14}-C_{19}-H_{24}	-179.32	-179.31
C_{14}-C_{15}-C_{16}-C_{17}	-0.01	-0.04
C_{14}-C_{15}-C_{16}-H_{21}	179.96	179.95
H_{20}-C_{15}-C_{16}-C_{17}		
H_{20}-C_{15}-C_{16}-H_{21}		

	C_{15}-C_{16}-C_{17}-C_{18}
	C_{15}-C_{16}-C_{17}-H_{22}
	H_{21}-C_{16}-C_{17}-C_{18}
	H_{21}-C_{16}-C_{17}-H_{22}
	C_{16}-C_{17}-C_{18}-C_{19}
	C_{16}-C_{17}-C_{18}-H_{23}
	H_{22}-C_{17}-C_{18}-C_{19}
	H_{22}-C_{17}-C_{18}-H_{23}
	C_{17}-C_{18}-C_{19}-C_{14}
	C_{17}-C_{18}-C_{19}-H_{24}
	H_{23}-C_{18}-C_{19}-C_{14}
	H_{23}-C_{18}-C_{19}-H_{24}

4.1. Vibrational Analysis

The title molecule consists of 26 atoms, which undergo 72 normal modes of vibrations. On the basis of C_1 symmetry the 72 fundamental vibrations of the title molecule can be distributed into 49 in-plane and 23 out-of-plane vibrations of same species. FT-IR and FT-Raman spectral wavenumbers have been assigned to base on the normal coordinate analysis following the scaled quantum mechanical force field methodology.The output files of the quantum chemical calculations contain the force constant matrix in Cartesian co-ordinates and in Hartree/Bohr^2 units. The force constants are transformed to the force fields in the local symmetry coordinates. The spectroscopic signature of 4PMP, a frequency calculation is performed on the gaseous phase of the molecule, while experimental FT-IR and FT-Raman are performed on the solid phase of the molecule. Hence there are disagreements between calculated and observed vibrational wavenumbers. To overcome discrepancies between observed and calculated wavenumbers, the scaling factors have been introduced by using a least square optimization method. To calculate optimal scaling factors (λ), we employed at least-square procedure using the following equation [9]

$$\left[\lambda = \frac{\sum_i^{all} \omega_i^{theory} v_i^{\exp t}}{\sum_i^{all} \left(\omega_i^{theory} \right)^2} \right]$$

where ω_i^{theory} and $V_i^{\exp t}$ are the ith theoretical harmonic and ith experimental fundamental frequencies (in cm^{-1}), respectively. Only single (uniform) scaling factors were calculated, without discrimination for different vibrations. The value obtained is 0.9621 for B3LYP and o.9617 for 6-31+G (d) and 6-311++G (d, p) methods and it is very close to the recommended scaling factor of 0.962 The root mean square (RMS) value is obtained in the study using the following expression:

$$\left[RMS = \sqrt{\frac{1}{n-1} \sum_i^n \left(v_i^{cal} - v_i^{\exp} \right)^2} \right]$$

The RMS error between unscaled and experimental frequencies is found 113 cm^{-1} by B3LYP/6-31+G (d)and 6-311++G (d, p) 96 cm^{-1} by /6-311G++ (d, p) levels. However, for reliable information's on the vibrational properties the use of a selective scaling is necessary. Figs. 5 and 6 present the experimental and calculated FT-IR and FT-Raman spectra for comparative purposes. The resulting vibrational wavenumbers for the optimized geometry and the proposed vibrational assignments as well as IR and Raman intensities are summarized in Table 3.

Ring Vibrations

Ring vibrational modes are sensitive to substitutions. Owing to aromatic ring vibrations, phenols absorb strongly in the region 1600−850 cm^{-1} .The ring stretching vibrations are very prominent, as the double bond is in conjugation with the ring, in the vibrational spectra of benzene and its derivatives [10]. The carbon−carbon stretching vibrations occur in the region of 1650−1200 cm^{-1}. In general, the bands are of variable intensity and are observed at 1625−1590, 1590−1575, 1540−1470, 1465−1430 and 1380−1280 cm^{-1} from the frequency ranges given by Varsanyi [11] for the five bands in the region. In the present work, the frequencies observed in FT-IR spectrum at 1616, 1604, 1511, 1465, 1325 and 1220 cm^{-1} have been assigned to C−C stretching vibrations. The corresponding vibration appears in FT-Raman spectrum at 1614, 1464 and 930 cm^{-1}. Theoretically computed values calculated at 1628, 1615, 1576 and 1282 cm^{-1} and by B3LYP/6-31+G (d) and B3LYP/6-311++G (d, p) methods. These are shows excellent agreement with experimental data's. The C−C−C in-plane bending vibrations are always occurs below 700 cm^{-1}, these bands are quite sensitive to change in the nature and position of the substituent's [12]. In 4PMP, the C−C−C in-plane bending vibrations observed at FT-IR 742, 702, and 686cm^{-1} in FT-Raman and predicted C−C−C out-of-plane bending vibrations are also in good agreement with the measured values. The ring torsion was calculated at 55 and 57 cm^{-1} in B3LYP/6-31+G (d) and B3LYP/6-311++G (d, p) methods, respectively.

O−H Vibrations

The O−H group gives rise to three vibrations such as stretching, in-plane bending and out-of-plane bending vibrations. The O−H group vibrations are likely to be the most sensitive in the environment, so they show pronounced shifts in the spectra of the hydrogen bonded species. The O−H stretching vibration is normally observed in the region around 3500 cm^{-1} [13]. In the present case, a medium-strong broad absorption at 3272 cm^{-1} in FT-IR and 3272 cm^{-1} in FT-Raman spectrum are assigned to O−H stretching vibration. The stretching vibrational wavenumber of free O−H is practically unchanged, while that of the bond O−H is red shifted. The red shift of the O−H stretching wavenumber is due to the formation of strong O−H$_{...}$O hydrogen bonds by hyper-conjugation between aldehydic oxygen lone electron pairs and O−H anti-bonding orbital's. The in-plane bending of O−H vibrations observed in the region 1250−1150 cm^{-1} [14] taken as the second criterion. This is evident for the absorption at 1175cm^{-1} is nearly correlated with experimental spectrum. The out-of-plane bending vibrations are usually occurring in the region 720-590cm^{-1} [15]. In 4PMP, out-of-plane bending vibrations are found at 652cm^{-1} in FT-Raman spectrum. These assignments are validated by the literature.

C−O Vibrations

The C−O stretching vibrations in alcohol and phenol produce a strong band in the region 1260−1000 cm^{-1} [16]. In present case, a medium FT-IR spectrum at 1248 cm^{-1} has been assigned to C−O stretching vibration. The corresponding vibration appears in the FT-Raman spectrum at 1072, 1037 cm^{-1}. The theoretically computed values of B3LYP level are 1248cm^{-1} and the bands of level are at 1038 cm^{-1}. These are shows excellent agreement with experimental data's. The in-plane bending vibration often occurs with sharp and strong intense band in and FT-Raman bands observed at 446 and 415 cm^{-1}. The theoretically computed values are at 925 cm^{-1} shows good agreement with experimental values. The calculated out-of-plane bending vibrations are computed at 262cm^{-1} by B3LYP method with 6-31+G (d) and 6-311G++ (d, p) basis sets, respectively.
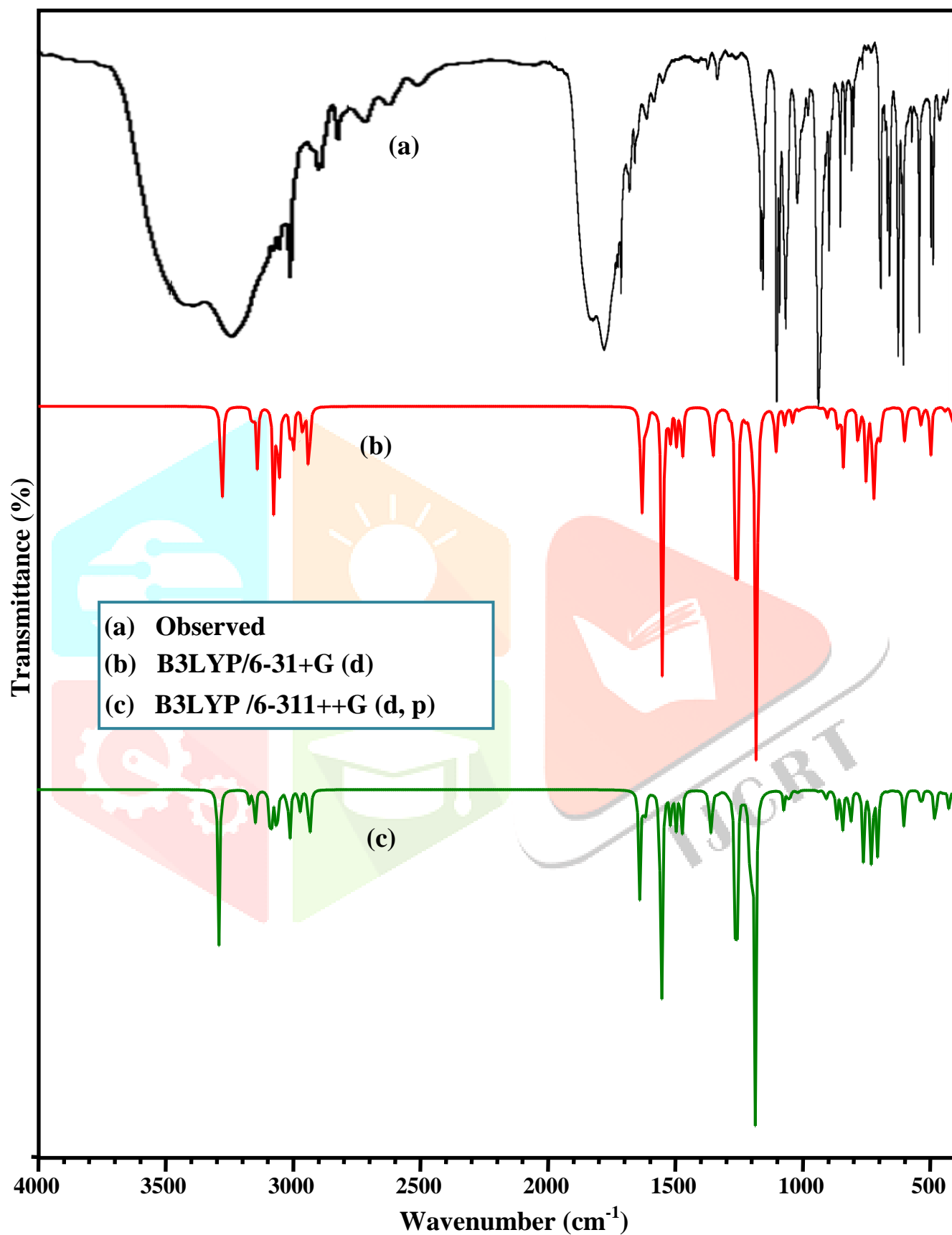
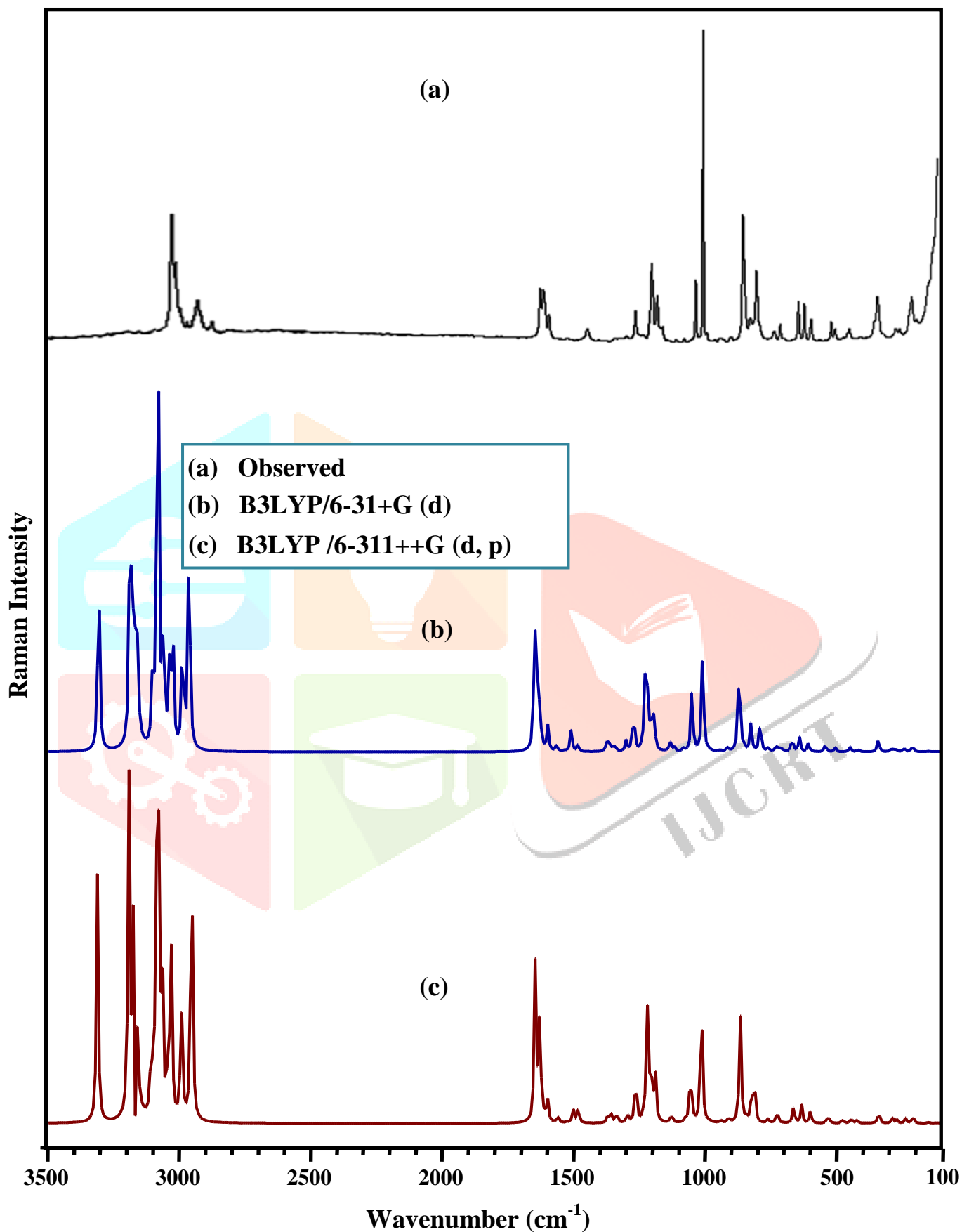Fig. 5. Observed and calculated FT-IR spectra of 4-(phenylmethyl) phenol

Fig.6. Observed and calculated FT-Raman spectra of 4-(phenylmethyl) phenol

Table 3

Vibrational assignments of FT-IR and FT-Raman peaks along the theoretically computed wavenumbers, IR intensity (I_{IR}) and Raman intensity (I_{Raman}) and the percentage of potential energy distribution.

S.No	Observed wave number (cm-1)		Calculated wave number (cm^{-1})								Assignments with(%) of PED[c]
	FT-IR	FT-Raman	B3LYP/6-31+G (d)				B3LYP/6-311G$_{++}$(d,p)				
			Unscaled	Scaled	I_{IR}	I_{Raman}	Unscaled	Scaled	I_{IR}	I_{Raman}	
1	3272		3753	3279	52.78	132.68	3837	3284	67.39	129.25	υOH(98)
2			3210	3160	8.74	179.09	3192	3165	6.14	178.22	υCH(97)
3			3205	3140	22.94	324.75	3188	3142	17.59	322.72	υCH(96)
4	3068		3193	3075	41.32	34.81	3176	3080	31.27	33.09	υCH(97)
5			3188	3061	10.77	87.91	3170	3062	7.72	87.88	υCH(98)
6			3186	3053	10.70	120.11	3168	3051	8.22	113.20	υCH(97)
7	3045		3177	3052	13.26	72.26	3160	3057	10.51	68.99	υCH(96)
8		3026	3176	3033	2.19	78.44	3159	3038	1.43	75.49	CH$_2$Sciss(92)
9			3169	3012	9.55	41.84	3153	3015	7.56	35.84	υCH(95)
10		2992	3162	2999	23.79	83.64	3146	3004	19.85	78.54	υCH(94)
11	2962	2954	3061	2961	13.33	65.33	3051	2966	11.40	61.88	υCH(93)
12	2930		3030	2937	32.82	145.99	3020	2927	28.66	152.45	CH$_2$Sciss(91)
13		1628	1666	1630	48.10	55.80	1654	1628	46.90	54.63	υCC(85)
14	1616	1615	1655	1617	6.28	35.59	1642	1613	6.71	34.07	υCC(87)
15	1604		1643	1608	9.98	9.05	1632	1603	9.72	8.80	υCC(90)
16		1576	1634	1580	0.59	10.03	1622	1582	0.59	9.32	υCC(89)
17			1556	1547	106.26	2.31	1543	1542	112.5	2.10	υCC(90)
18	1511		1538	1518	14.97	0.47	1525	1506	16.89	0.42	υCC(87)
19	1488		1503	1492	13.75	8.20	1487	1484	16.65	4.39	CH$_{2Sciss}$(86)
20	1465		1492	1466	3.13	2.58	1477	1466	2.93	5.10	υCC(77)
21			1476	1470	19.45	0.47	1464	1461	18.46	0.64	υCC(80)
22			1378	1358	6.65	3.79	1365	1356	4.70	1.73	υCC(83)
23	1348		1374	1350	17.08	2.22	1361	1347	17.54	1.20	CH$_{2Wagg}$(86)
24			1366	1344	6.99	1.92	1352	1340	4.86	2.53	υCC(76)
25	1325		1361	1328	1.05	3.18	1343	1320	1.83	3.70	υCC(74)
26		1282	1318	1284	2.27	4.08	1302	1279	1.53	3.19	υCC(73)
27	1248	1253	1287	1256	127.48	16.84	1275	1248	127.9	17.09	υC-O(72)
28	1220		1230	1222	3.16	2.42	1222	1219	2.77	2.83	υCC(77)
29			1217	1211	0.17	22.49	1210	1204	0.06	30.98	υCC(80)
30			1211	1206	4.75	21.27	1204	1200	2.25	8.67	βCH(56)
31	1197	1200	1210	1193	12.07	8.37	1200	1189	26.92	9.93	βCH(58)
32			1205	1187	5.70	5.05	1195	1182	3.89	4.15	βCH(57)
33		1175	1195	1178	161.13	13.87	1186	1173	151.4	15.27	βO-H(67)
34	1116		1137	1118	0.40	3.95	1131	1172	0.05	3.03	βCH(60),υCC(12)
35	1096	1100	1131	1102	20.51	2.00	1123	1197	19.74	1.69	βCH(56),υCC(10)
36	1058	1062	1089	1066	8.22	1.24	1080	1060	8.57	1.02	βCH(60),υCC(7)
37	1034	1028	1054	1035	6.13	21.58	1050	1040	6.62	18.68	βCH(55),υCC(11)
38	988	1012	1032	1009	2.02	0.25	1030	1007	1.60	0.14	βCH(45),υCC(12)
39		987	1016	994	0.47	39.24	1017	999	0.26	43.07	βCH(44),βCC(7)
40			999	987	0.13	0.26	999	986	0.12	0.30	γCH(43), βCC(9)
41			978	970	0.04	0.25	982	968	0.06	0.29	γCH(46),βCC(7)
42			967	960	0.14	0.05	968	960	0.11	0.03	γCH(48),βCC(7)
43	900	925	955	928	0.83	0.56	952	926	0.86	0.71	β C-O(58)
44	895		943	904	1.04	0.57	941	898	1.03	0.77	γCH(48),βCC(7)
45			914	899	3.79	0.88	910	894	4.30	0.80	γCH(47),βCC(9)
46			861	857	11.80	32.48	859	853	12.67	32.16	γCH(48),βCC(10)
47	834		858	850	0.56	3.01	855	847	0.32	1.86	γCH(49)
48	808	832	851	837	23.59	1.24	849	830	21.10	1.52	γCH(47)

49		810	825	812	0.41	9.22	822	808	1.85	10.31	γCH(46)
50	742	775	814	777	18.83	11.96	812	778	16.29	9.56	CH$_{2roCK}$(66)
51		740	761	746	33.65	1.28	762	747	32.63	1.16	βCC(49)
52	702	715	738	718	40.02	1.75	738	717	31.05	1.47	βCC(48)
53	686		711	704	15.44	1.88	717	710	6.31	2.10	βCC(41)
54			706	690	13.07	0.53	711	699	29.76	0.07	βCCC(46)
55		652	656	656	0.52	5.06	656	650	0.54	5.18	γO-H(43)
56		625	634	629	0.25	4.93	635	620	0.26	5.09	βCH
57	592	589	607	594	16.18	3.24	608	587	16.83	3.29	βCH
58		525	532	530	8.50	2.28	530	520	2.41	527.01	γCCC
59	468	468	483	493	19.27	1.43	484	465	19.65	1.12	γCCC
60	433		442	437	1.70	1.59	444	432	1.76	1.55	γCCC
61			423	410	0.34	0.10	422	413	0.87	0.08	CH$_2$ twist(44)
62			420	407	9.49	0.74	421	410	9.11	0.79	γCCC
63		350	357	344	0.11	0.08	358	347	0.09	0.06	γCCC
64			340	330	18.60	4.14	340	328	5.23	3.37	γCCC
65		275	296	280	96.41	1.29	289	277	4.23	1.37	γCCC
66		262	281	264	1.36	1.04	276	260	100.9	0.94	γC-O(43)
67		225	237	232	0.57	1.39	230	227	0.61	1.40	γCCC
68		196	204	200	1.68	2.05	204	197	1.66	2.00	γCCC
69			145	143	0.77	0.17	144	140	0.86	0.15	γCCC
70			53	52	0.21	7.08	54	52	0.19	6.81	γCCC
71			29	28	0.28	7.39	31	29	0.23	7.38	γCCC(47)
72			24	23	0.59	3.93	24	23	0.58	3.78	γ CCC(41)

ass – asym stretching, ss – sym stretching, ipb – in-plane-bending, opb – out-of-plane bending, sb – symd bending, ipr – in-plane rocking, opr – out-of-plane rocking, sciss – scissoring, rock – rocking, wagg – wagging, twist – twisting. Assignments: *ν* - stretching, *β* - in-plane bending, γ- out-of-plane bending

C−H Vibrations

The aromatic C−H stretching vibrations of hetero aromatic structures are expected to appear in the region 3100-3000 cm^{-1} [17]. The nature of substituent's can not affect the bands much in the region. In the present study, 3068, 3045, and 2962, cm^{-1} was assigned to C−H stretching vibration in FT-Raman spectrum. They show good agreement with theoretically computed values at 3200, 3102 and 3052 cm^{-1} in B3LYP and at 3192, 3093 and 3041 cm^{-1} in methods using 6-311G++ (d, p) basis set. The observed wavenumbers of C−H stretching vibrations are also in good agreement with the measured values and literature data [18]. The C−H in-plane and out-of-plane bending vibrations generally lie in the region 1300−1000 cm^{-1} and 1000−675 cm^{-1} [19], respectively. In accordance with above literature data the weak band observed in FT-IR spectrum at 1197, 1116, 1096, 1058, 1034,and 988 cm^{-1} in FT-Raman spectra. The weak to strong FT-IR bands observed at 900, 895,834, and 808 cm^{-1} and FT-Raman bands observed at 625cm^{-1} are assigned to C−H out-of-plane bending vibration. They are good agreement with literature values [20]. The B3LYP and calculated wavenumbers at are correlated with experimental values.

CH$_2$ Vibrations

For the assignments of CH$_2$ group frequencies basically Six fundamental can be associated to each CH$_2$ group namely CH$_2$ symmetric stretch, CH$_2$ asymmetric stretch, CH$_2$ Scissoring and CH$_2$ rocking which belongs to in-plane bending vibrations and to out of plane bending vibrations, viz., CH$_2$ asymmetric stretching vibrations are generally observed in the region 3000−2900 cm^{-1}, while the CH$_2$ symmetric stretching vibrations were appearing between 2900−2800 cm^{-1}.[21] For our title compound, the CH$_2$ asymmetric and symmetric stretching vibrations are observed at

3026 and 2930cm^{-1} in FT-Raman Spectrum. The calculated asymmetric and symmetric CH$_2$ stretching vibrations are 3068, 2992, and 2994cm^{-1} at FT-IR and FT-Raman spectra of 4PMP.

In the present study, the CH$_2$ bending modes follow, in decreasing wave number, the general order CH$_2$ scissoring > CH$_2$ wagging > CH$_2$ twisting > CH$_2$ rocking. Since the bending modes involving hydrogen atoms attached to the control carbon atom falls into the 1450−875 cm^{-1} range, there is extensive vibrational coupling of these modes with CH$_2$ deformations particularly with the CH$_2$ twist. It is notable that with CH$_2$ scissoring and rocking wave sensitive to the molecular conformations.

The four bending modes of CH$_2$ groups are scissoring, rocking, wagging and twisting for EPAP molecule, are assigned to within the range. The CH$_2$ scissoring mode identified at 1488 cm^{-1} in FT-IR and CH$_2$ wagging mode observed at 1348 cm^{-1} in FT-Raman spectrum [22]. The peaks observed at 934 cm^{-1} in both spectra is assigned to CH$_2$ rocking, which is coupled with C−C stretching vibration and CH$_2$ twisting mode observed at 423 cm^{-1} in FT-IR spectrum. All these calculated values are in good agreement with the observed values.

4.2. Mulliken Atomic Charges

The Mulliken atomic charges calculation has an important role in the application of quantum mechanical calculations to molecular system [23] because of atomic charges effect dipole moment, molecular polarizability, electronic structure and more a lot of properties of molecular systems. Mulliken atomic charges calculated at the DFT/B3LYP/6-31+G (d) and /6-311++G (d, p) methods is presented in Table 4.

Table 4

Mulliken's population analysis of 4-(phenylmethyl)phenol performed at B3LYP/6-31+G (d) and B3LYP/6-311++G (d, p) methods.

S. No.	Atom No.	Mulliken's Atomic charges	
		B3LYP/6-31+G (d)	B3LYP/6-311++G (d, p)
1	C_1	0.1253	-0.4518
2	C_2	0.0117	-0.0142
3	C_3	-0.5956	-0.5670
4	C_4	0.7561	1.3347
5	C_5	-0.5558	-0.3802
6	C_6	0.0538	-0.2487
7	O_7	-0.6813	-0.2367
8	H_8	0.4729	0.2614
9	H_9	0.1649	0.1449
10	H_{10}	0.1860	0.1633
11	C_{11}	-1.0568	-1.0453
12	H_{12}	0.2117	0.1746
13	H_{13}	0.2139	0.1745
14	C_{14}	0.6283	1.3036
15	C_{15}	-0.1997	-0.4250
16	C_{16}	-0.2318	-0.2735
17	C_{17}	-0.1503	-0.3593
18	C_{18}	-0.3541	-0.2762
19	C_{19}	-0.2474	-0.4318
20	H_{20}	0.1681	0.1463
21	H_{21}	0.1778	0.1728
22	H_{22}	0.1766	0.1441

23	H_{23}	0.1784	0.1787
24	H_{24}	0.1850	0.1616
25	H_{25}	0.1714	0.1544
26	H_{26}	0.1910	0.1946

It is worthy to mention that C_4 atom is more acidic due to more positive charge. The Mulliken atomic charges of the phenol group hydrogen atom H_8 are higher than the aromatic group and methyl group hydrogen. It denotes that the phenol group hydrogen atoms are more acidic than the aromatic and methyl group hydrogen atoms, however that the high value 0.862808 and 0.593193e for C_4 in B3LYP and methods with 6-31+G (d) and 6-311++G (d, p) basis set. The O_7 atom exhibit high negative charge is -0.696869 and -0.266469 for B3LYP method with 6-31+G (d) and 6-311++G (d, p) basis sets. The results can however better represent in graphical 3D form as given Fig. 7, respectively.
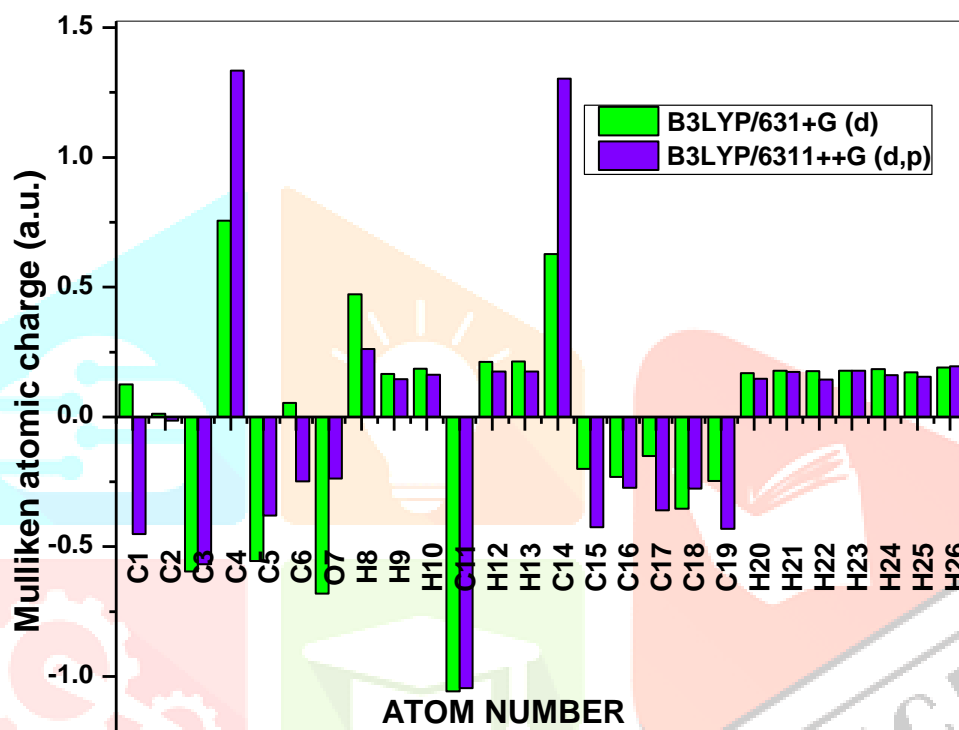

Fig. 7. Comparative Mulliken's plot by B3LYP/6-31+G (d) and B3LYP/6-311++G (d, p) Level 4-phenylmethyl) Phenol

4.3. HOMO-LUMO analysis

The most important Frontier molecular orbital (FMO) such as highest occupied molecular orbital (HOMO) and lowest unoccupied molecular orbital (LUMO) plays a crucial part in the chemical stability of the molecule [24]. The HOMO represents the ability to donate an electron and LUMO represents the ability of accept an electron. The energy gap between HOMO and LUMO also determines the chemical reactivity, optical polarizability and chemical hardness– softness of a molecule. A molecule with a small frontier orbital gap is more polarizable and is generally associated with a high chemical reactivity, low kinetic stability and is also termed as soft molecule [25].

According to the results, the 4PMP contains 47 occupied molecular orbitals and 339 unoccupied molecular orbitals. The HOMO and LUMO energies calculated at B3LYP method with 6-31+G (d) and 6-311++G (d, p) basis set are presented in Table 5. The HOMO and LUMO pictures and their orbital energies are calculated by B3LYP/6-31+G (d) and 6-311++G (d, p) are shown in Fig.8, respectively. The positive phase is red and negative one. It is clear from the Fig. 8, shows that the isodensity plots for the HOMO and LUMO are well localized and the intra-molecular interactions

mostly occurred within the ring. The transition HOMO-LUMO which has a relative energy gap of 6.824 eV and 6.328 eV in B3LYP method with 6-31+G (d) and 6-311++G (d, p) basis sets, respectively.

Table 5

Comparison of HOMO, LUMO energy gaps and related molecular properties of 4-(phenylmethyl) phenol at B3LYP/6-31+G (d) and B3LYP/6-311++G (d, p) methods.

| Molecular properties	Energy (a.u.)	Energy gap (eV)	Ionization potential (I)	Electron affinity (A)	Global Hardness (n)	Electro negativity (χ)	Global softness (υ)	Chemical potential (μ)	Global Electrophilicity (ω)
B3LYP/6-31+G(d)									
HOMO	-0.22674	6.824	-0.22674	-0.02404	0.10135	0.12539	9.86679	-0.12539	0.08666
LUMO	-0.02404								
B3LYP /6-311++G(d, p)									
HOMO	0.22912	6.328	0.22912	0.00343	0.112845	0.1162	8.86171	-0.1162	0.05981
LUMO	0.00343								
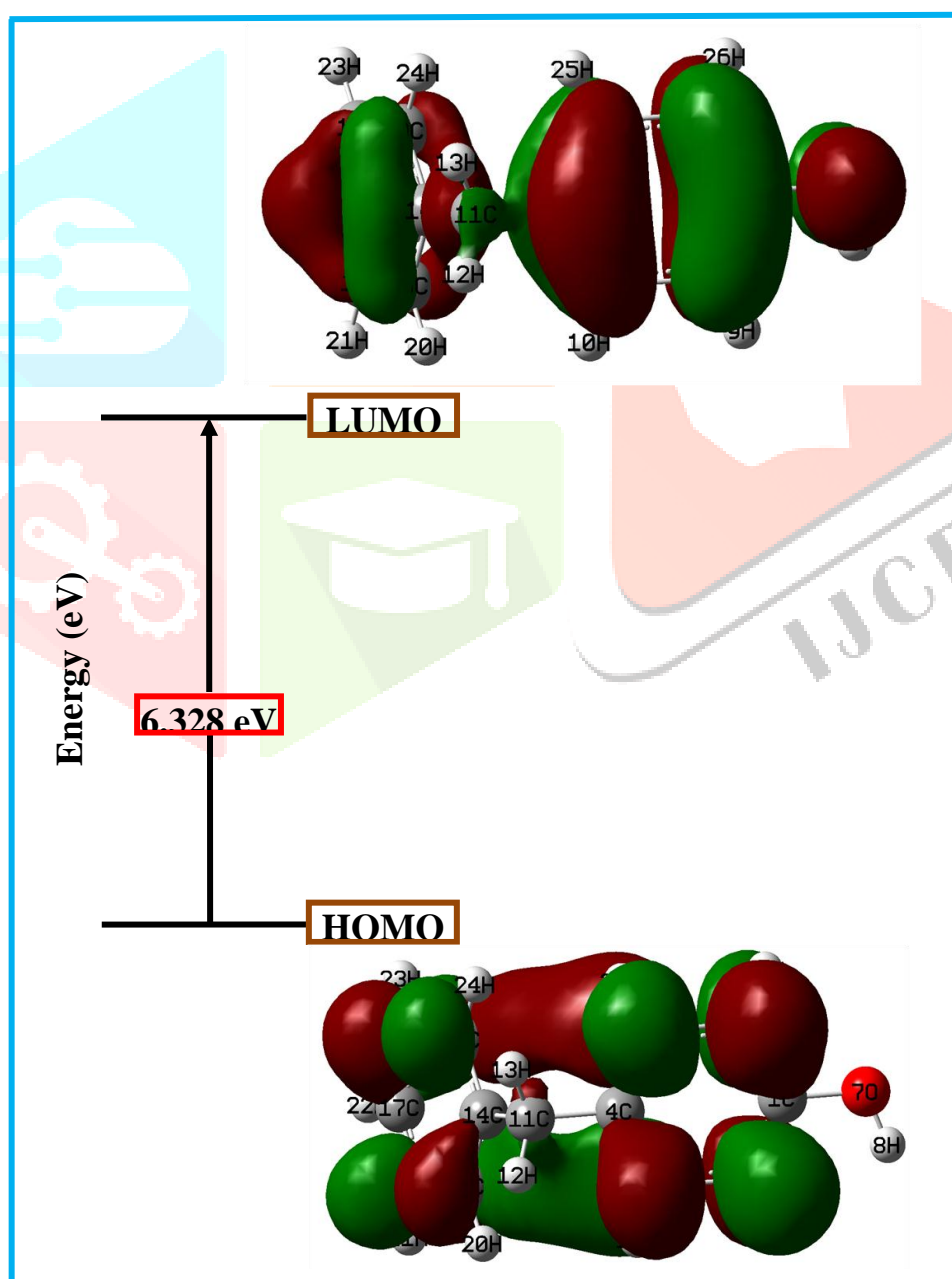
Fig. 8. The molecular orbitals and energies for the HOMO and LUMO of 4-(phenylmethyl) phenol

Global reactivity descriptorS

Based on the density functional descriptors, global chemical reactivity descriptors of title molecule such as ionization potential (I), electron affinity (A), chemical potential (μ), electronegativity (χ), global hardness (η), global softness (σ) and global electriphilicity (ω) values can be described as followed [26]. In simple molecule orbital theory approaches, the HOMO energy (E_{HOMO}) is related to the ionization potential (I) by Koopman's theorem and LUMO energy (E_{LUMO}) has been used to estimate the electron affinity (A) [27].

$$\left[\begin{array}{l} \text{Ionization potential (I)} = -E_{HOMO} \\ \text{Electron affinity (A)} = -E_{LUMO} \end{array}\right]$$

The average value of the HOMO and LUMO energies is related to the electronegativity (χ) defined by Mulliken [23].

$$\left[\text{Electronegativity}\,(\chi) = \frac{(I+A)}{2}\right]$$

In addition, the HOMO and LUMO energy is related to the hardness (η) and softness (σ) [28].

$$\left[\begin{array}{l} \text{Global hardness}\,(\eta) = \dfrac{(I-A)}{2} \\ \text{Global softness}\,(\sigma) = \dfrac{1}{\eta} \end{array}\right]$$

Parr et al. [29] defined global electriphilicity (ω)

$$\left[\text{Electriphilicity}\,(\omega) = \frac{\mu^2}{2\eta}\right]$$

where μ is the chemical potential takes the average value of ionization potential (I) and electron affinity (A) [30].

$$\left[\text{Chemical potential}\,(\mu) = -\frac{(I+A)}{2}\right]$$

The electronic chemical potential is the parameter which describes the escaping tendency of electrons from an equilibrium system. Thus the frontier molecular orbital analysis also provided the details on chemical stability, chemical hardness and electronegativity of the molecule in B3LYP/6-31+G (d) and B3LYP/6-311++G (d, p) methods are presented in Table 5, respectively.

4.5. Molecular electrostatic potential (MEP)

At any given point $r(x, y, z)$ in the vicinity of a molecule, the molecular electrostatic potential, $V(r)$ is defined in terms of the interaction energy between the electrical charge generated from the molecule electrons and nuclei and a positive test charge (a proton) located at r [31]. The molecular electrostatic potential (MEP) is related to the electron density and a very useful descriptor for determining sites for electrophilic and nucleophilic attack as well as hydrogen-bonding interactions [32]. For the systems studied the molecular electrostatic potential values were calculated as described using the equation:

$$V(r) = \sum \frac{Z_A}{|R_A - r|} - \int \frac{\rho(r')}{|r' - r|} dr$$

where the summation runs over all the nuclei A in the compound and polarization and reorganization effects are neglected. Z_A is the charge of the nucleus A, located at R_A and $\rho(r')$ is the electron density function of the molecule. The molecular electrostatic

potential MEP map for positive and negative sites of the title molecule as shown in Fig.9. The MEP is a plot of electrostatic potential mapped onto the constant electron density surface. Different values of the electrostatic potential are represented by different colors. Red represents the regions of the most negative electrostatic potential and blue represent the regions of the most positive electrostatic potential. Potential increases in the order red < orange < yellow < green < blue. The color grading of resulting surface simultaneously displays molecular size, shape and electrostatic potential value which are very useful in research of molecular structure with its physiochemical property relationship [33]. It is clear from the figure, while regions having the negative potential are over the electronegative atoms (oxygen atoms), the regions having the positive potential are over the hydrogen atoms. As can be seen from the MEP of the title molecule, more reactive sites are near O−H group, the regions having the most negative potential over the oxygen atoms C_{19} the negative potential values are -14.7385 a.u. indicates the strongest repulsion (electrophilic attack). A most positive region localized on the hydrogen atoms C_4 and its values are 0.33180 a.u. indicates the strongest attraction (nucleophilic attack), respectively.

| Charges (e)	Atoms	V (r) (a.u.)
-0.6503	O_7	22.2743
-0.3267	C_{19}	14.7385
-0.3055	C_{15}	14.7382
-0.1910	C_{17}	14.7378
-0.6501	C_{18}	14.7356
-0.0738	C_{16}	14.7356
-0.2033	C_6	14.7334
-0.3097	C_5	14.7324
-0.2291	C_3	14.7313
-0.3296	C_2	14.7299
-0.5456	C_{11}	14.7292
0.3318	C_4	14.7283
0.3995	C_{14}	14.7269
0.4106	C_1	14.6675
0.1437	H_{12}	1.1113
0.1528	H_{13}	-1.1113
0.1304	H_{22}	-1.1068
0.1126	H_{23}	-1.1053
0.1196	H_{21}	-1.1051
0.1602	H_{24}	-1.1032
0.1511	H_{20}	-1.1029
0.1738	H_{26}	-1.1004
0.1714	H_{25}	-1.1098
0.1614	H_{10}	-1.1097
0.1648	H_9	-1.0882
0.4310	H_8	-1.9645
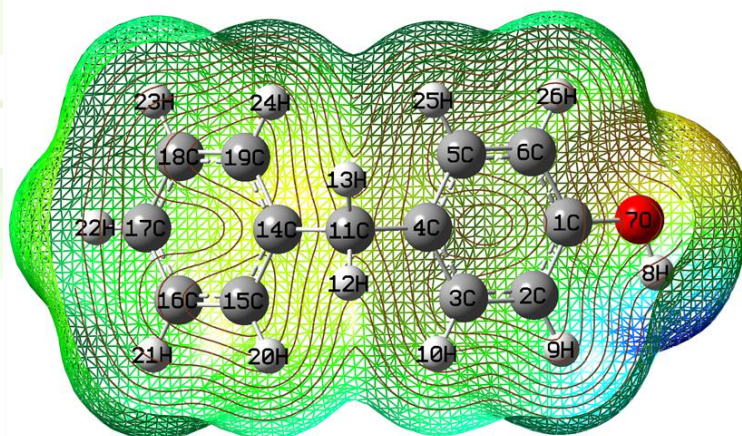
Fig. 9. Calculated 3D molecular electrostatic potential contour map of 4-(phenylmethyl) phenol

5. CONCLUSION

In the present work, the optimized molecular structure of the stable conformer, electronic properties, vibrational frequencies and intensity of vibrations of the title compound have been calculated by DFT/B3LYP/6-31+G (d) and DFT/B3LYP/6-311++G(d, p) methods level calculations. The optimized geometric parameters (bond lengths and bond angles) are theoretically determined and compared with the experimental results. The vibrational FT-IR and FT-Raman spectra of the 4PMP are recorded and on the basis of agreement between the calculated and experimental results. The frontier molecular orbital's (FMOs) and HOMO−LUMO analysis are industrially important of the molecule. The calculated HOMO−LUMO and frontier orbital energy gap values along with their 3D plot are presented in this study for better understanding of charge transfer occur within the molecule the first order hyperpolarizability value of the title compound is approximately 1.36 and 1.46 times greater than the value of urea in both basis sets. The MEP map shows the negative potential sites are on oxygen and hydrogen atoms as well as the positive potential sites on the molecule.

REFERENCES

[1] M.J. Frisch, et al., GAUSSIAN 09, Revision A. 9, Gaussian, INC, Pittsburgh, 2009.

[2] H.B. Schlegel, *J. Comput. Chem.* 3, 1982, 214−218.

[3] E.D. Glendening, A.E. Reed, J.E. Carpenter, F. Weinhold. NBO Version 3.1.TCI. University of Wisconsin, Madison, 1998.

[4] T. Sundius, *J. Mol. Struct.* 218, 1990, 321−326; MOLVIB: A Program for Harmonic force field calculations. QCPE Program No. 807, 2002.

[5] P.L. Polavarapu, *J. Phys. Chem.* 94, 1990, 8106−8112.

[6] G. Keresztury, BT Raman spectroscopy. Theory, in: J.M. Chalmers, P.R. Griffiths (Eds.), Handbook of Vibrational Spectroscopy, Vol. 1, John Wiley & Sons Ltd., 2002, 71−87.

[7] X. Sun, Q. Zhao, X.W. Wei, Z.Y. Yu, D. Li, X. Wang, Y.S. Wang. *J. Mol. Struct. (Theochem.),* 74, 2009, 901−904.

[8] D.A. Kleinman, *Phys. Rev.* 126, 1962, 1977−1979.

[9] P. Pulay, G. Fogarasi, F. Pong. J.E. Boggs. *J. Am. Chem. Soc.* 101, 1979, 2550−2560.

[10] G. Varsanyi, Vibrational Spectra of Benzene Derivatives, Academic Press, New York, 1969.

[11] G. Varsanyi, Assignments of Vibrational Spectra of Seven Hundred Benzene Derivatives, Vols. 1–2, Adam Hilger, 1974.

[12] R.J. Jakobsen, F.F. Bentley, *Appl. Spectrosc.* 18, 1964, 88–92.

[13] S. Bratoz, D. Hadzi, N. Sheppard, *Spectrochim. Acta A* 8, 1956, 249−261.

[14] D. Michalska, D.C. Bienko, A.J.A. Bienko, Z. Latajaka, *J. Phys. Chem.* 100, 1996, 1186−1193.

[15] S. Ahmad, S. Mathew, P.K. Verma, *Indian J. Pure Appl. Phys.* 30, 1992, 764– 770.

[16] M. Kubinyi, F. Billes, A. Grofcsik, G. Keresztury, *J. Mol. Struct.* 266, 1992, 339– 344.

[17] R.L. Peesole, L.D. Shield, I.C. McWilliam, Modern Methods of Chemical Analysis, Wiley, New York, 1976.

[18] G. Santhi, V. Balachandran, V. Karpagam, *Elixir Vib. Spec.* 36, 2011, 3373−3387.

[19] A. Altun, K. Golcuk, M. Kumru, *J. Mol. Struct. (Theochem.)*, 155, 2003, 637–639.

[20] V. Krishnakumar, V. Balachandran, *Spectrochim. Acta Part A* 63, 2006, 464−476.

[21] Sajan D., J. Binoy, B. Pradeep, K. Venkatakrishnan, V. Kartha, I. Joe, V.Jayakumar, 2004. Spectrochim. Acta Part A 60: 173–180.

[22] Wiberg K.B., A. Sharke, S. Sampathkrishnan, 2011. Mol. Simul. 37: 1276–1288.

[23] R.S. Mulliken, *J. Chem. Phys.* 2, 1934, 782−793.

[24] S. Saravanan, V. Balachandran, K. Viswanathan, *Spectrochim. Acta Part A* 12, 2014, 685−697.

[25] B.J. Powell, T. Baruah, N. Bernstein, K. Brake, R.H. McKenzie, P. Meredith, M.R. Pederson, *J. Chem. Phys.* 120, 2004, 8608–8615.

[26] S. Saravanan, V. Balachandran, *Spectrochim. Acta Part A* 120, 2014, 351−364.

[27] P. Politzer, F. Abu-Awwad, *Theor. Chim. Acta* 99, 1998, 83−87.

[28] R.G. Pearson, Chemical hardness, John Wiley-VCH, Weinheim, 1997.

[29] R.G. Parr, L. von Szentpaly, S. Liu, *J. Am. Chem. Soc*. 121, 1999, 1922–1924.

[30] J. Padmanabhan, R. Parthasarathi, V. Subramanian, P.K. Chattaraj, *J. Phys. Chem*. A 111, 2007, 1358–1361.

[31] P. Politzer, J.S. Murray, The fundamental nature and role of the electrostatic potential in atoms and molecules, *Theor. Chem. Acc.* 108, 2002, 134–142.

[32] E. Scrocco, J. Tomasi, *Adv. Quantum Chem.* 11, 1978, 115–121.

[33] M. Szafran, A. Komasa, E.B. Adamska, *J. Mol. Struct. (Theochem.)* 827, 2007, 101–107.